

# Response of Ancillary Azide Ligand in Designing a 1D Copper(II) Polymeric Complex along with the Introduction of High DNA- and HAS-Binding Efficacy, Leading to Impressive Anticancer Activity: A Compact Experimental and Theoretical Approach

Manik Das, Somali Mukherjee,\* Md. Maidul Islam, Indranil Choudhuri, Nandan Bhattacharyya, Bidhan Chandra Samanta, Basudeb Dutta, and Tithi Maity\*



Cite This: *ACS Omega* 2022, 7, 23276–23288



Read Online

ACCESS |



Metrics & More

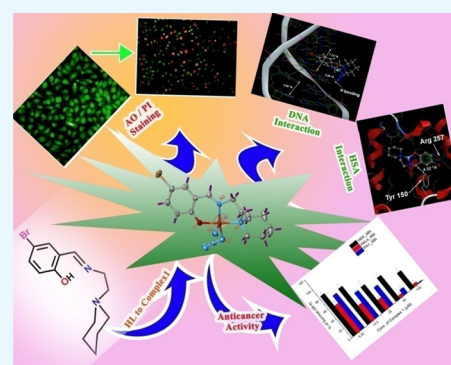


Article Recommendations



Supporting Information

**ABSTRACT:** A new versatile azide-bridged polymeric Cu(II) complex, namely,  $[\text{Cu}(\text{L})(\mu_{1,3}\text{-N}_3)]_{\infty}$  (**1**), was synthesized utilizing an N,N,O-donor piperidine-based Schiff base ligand (*E*)-4-bromo-2-((2-(-1-yl)imino)methyl)phenol (**HL**), obtained via the condensation reaction of 1-(2-aminoethyl) piperidine and 5-bromo salicylaldehyde. The single-crystal X-ray diffraction analysis reveals that complex **1** consists of an end-to-end azido-bridged polymeric network, which is further rationalized with the help of a density functional theory (DFT) study. After routine characterization with a range of physicochemical studies, complex **1** is exploited to evaluate its biomedical potential. Initially, theoretical inspection with the help of a molecular docking study indicated the ability of complex **1** to effectively bind with macromolecules such as DNA and the human serum albumin (HSA) protein. The theoretical aspect was further verified by adopting several spectroscopic techniques. The electronic absorption spectroscopic analysis indicates a remarkable binding efficiency of Complex **1** with both DNA and HSA. The notable fluorescence intensity reduction of the ethidium bromide (EtBr)–DNA adduct, 4',6-diamidino-2-phenylindole (DAPI)–DNA adduct, and HSA after the gradual addition of complex **1** authenticates its promising binding potential with the macromolecules. The retention of the canonical B form of DNA and  $\alpha$  form of HSA during the association of complex **1** was confirmed by implementing a circular dichroism spectral study. The association ability of complex **1** with macromolecules further inspired us to inspect its impact on different cell lines such as HeLa (cervical cancer cell), PA1 (ovarian cancer cell), and HEK (normal cell). The dose-dependent and time-dependent *in vitro* 3-(4,5-dimethylthiazol-2-yl)-2,5-diphenyltetrazolium bromide (MTT) assay suggests an effective antiproliferative property of complex **1** with low toxicity toward the normal cell line. Finally, the anticancer activity of complex **1** toward carcinoma cell lines was analyzed by nuclear and cellular staining techniques, unveiling the cell death mechanism.



## INTRODUCTION

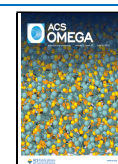
Metal complexes occupy a leading place in the drug development domain for the fabrication of new cancer therapeutics.<sup>1–4</sup> After the successful implementation of platinum-based anticancer drugs, inorganic medicinal chemistry has introduced a new class of therapeutic agents that are not fully accessible through organic chemistry.<sup>5–8</sup> However, the well-known drawbacks, such as low solubility, multifactorial resistance, high cost, and toxicity, restrict their global usability in chemotherapy.<sup>9–11</sup> In this context, among the series of bioessential metals, copper has been exposed as one of the best alternatives to platinum due to its important homeostatic and metabolic effects on all types of cancers along with specific responses toward malignant cells.<sup>12–17</sup> A large variety of copper complexes are already designed to be inspected as anticancer agents showing potential cytotoxicity in several *in vitro* and *in vivo* experiments involving a different mechanistic

pathway.<sup>18–21</sup> In most of these cases, DNA is found to be one of the main targets for cancer therapeutics, where the DNA–drug interactions hinder DNA replication, preventing the uncontrolled growth of malignant cells.<sup>22–27</sup> Consequently, to reduce the side effects of an anticancer drug molecule and to increase its specificity, a definite approach has frequently been implemented by the scientific community, where a fixed drug delivery vehicle, such as an antibody, peptide, protein, etc., is linked to the drug molecule. Among these, human serum albumin (HSA) is the most plentiful circulating protein in the

Received: March 8, 2022

Accepted: June 14, 2022

Published: June 28, 2022



human blood plasma, which can transport the drug molecule to the target location.<sup>28</sup> Drugs bound to HSA can reach target tissues without being exposed to normal cells, thus diminishing its toxic effect on healthy cells and tissues.<sup>29–31</sup> Thus, to implement a metal-based complex as an effective anticancer agent, the primary need is to investigate its interaction potential with DNA and HSA.

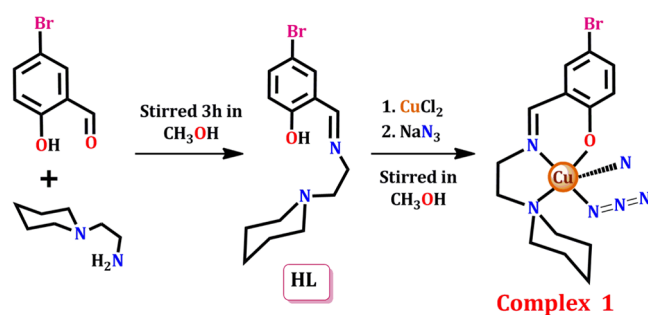
Furthermore, the choice of the ligand framework is of considerable importance as it can regulate the distribution of the complex in biological systems, in turn improving its efficiency.<sup>29</sup> Among several organic moieties, the N,N,O-donor Schiff bases have gained special recognition as they bear enhanced flexibility to hold the metal ions along with potential bioactivities, pharmacological activities, etc. However, the surprising fact is that N,N,O-donor Schiff bases derived from substituted piperidine are relatively less explored with regard to their DNA and HSA binding efficacy and anticancer properties. At the same time, different Schiff base–copper complexes (Table S1) have also been designed and exploited as efficient cancer therapeutics to date. Besides, the successful introduction of metal–azide complexes as potential anticancer agents without subsidiary toxicity to normal cell lines has inspired chemists to use azide as a secondary anionic agent.<sup>32,33</sup> Interestingly, in this developing research area, Schiff base complexes having a pendant or bridging azide ion hold a special position because of their high applicability (Table S2).

Addressing all of these points, in this study, we synthesized a new Cu(II) complex (**1**) derived from a piperidine-based Schiff base ligand, namely, (*E*)-4-bromo-2-((2-(1-yl)imino)methyl)phenol (**HL**). The azide anion was administered as a secondary anionic ligand to produce Cu(II) complexes of versatile nuclearity. The formation of polymeric complex **1** is well supported by theoretical computations. To analyze the biomedical application, the binding efficacy of complex **1** with ctDNA and HSA was thoroughly tested by the electronic spectroscopic technique (binding constant value  $2.265 \times 10^5 \text{ M}^{-1}$ ). The fluorometric titration of EtBr–DNA/DAPI–DNA adducts and HSA by the incremental addition of complex **1** shows an impressive fluorescence attenuation, with quenching constant values on the order of  $\sim 10^5$ , which suggests the efficient binding efficacy of complex **1** with macromolecules. Circular dichroism data show the retention of the configuration of DNA and HSA after association with complex **1**. The experimentally obtained findings match well with the prediction obtained by the molecular docking study. Finally, the anticancer activity of complex **1** was examined on HeLa (cervical cancer cell), PA1 (ovarian cancer cell), and HEK (normal) cell lines. The LD<sub>50</sub> values obtained from an *in vitro* 3-(4,5-dimethylthiazol-2-yl)-2,5-diphenyltetrazolium bromide (MTT) assay depict the effective anticancer property of complex **1** with low toxicity to the normal cell. In addition, the AO/PI staining technique is adopted to gain insights into the nuclear morphological changes and cell deformities of the aforementioned cell line after treatment with complex **1** in a dose-dependent manner.

## RESULTS AND DISCUSSION

**Synthesis, IR, UV, and ESI-MS Analysis of the Complexes.** Complex **1** was synthesized by reacting CuCl<sub>2</sub> with a Schiff base ligand (**HL**), developed by the association of 2-amino ethyl piperidine and 5-bromo salicylaldehyde followed by the addition of sodium azide (Scheme 1).

Scheme 1. Synthesis of Ligand HL and Complex 1



In the first step, the Fourier transform infrared (FT-IR) spectra of complex **1** are collected, which provide a prefatory idea regarding the existing bonds (Figure S1). In the case of complex **1**, the band at  $1636 \text{ cm}^{-1}$  indicates the presence of the characteristic C=N stretching of the imine bond. The sharp bands, centered at  $1310\text{--}1410 \text{ cm}^{-1}$ , indicate the vibration frequency of the benzene skeleton. The peaks at  $2032 \text{ cm}^{-1}$  and  $2075 \text{ cm}^{-1}$  provide authentic proof regarding the presence of the bridging azide in complex **1**. The UV–vis spectroscopic study of complex **1** is performed, which shows that complex **1** exhibits one absorption band at  $376 \text{ nm}$  ( $\epsilon = 11428 \text{ M}^{-1} \text{ cm}^{-1}$ ), which arises as a result of the CT transition. This band confirms the coordination of azomethine nitrogen and phenolato oxygen with the metal center. The appearance of an absorption band at  $650 \text{ nm}$  ( $\epsilon = 465 \text{ M}^{-1} \text{ cm}^{-1}$ ) in the visible region is attributed to the d–d transition (Figure S2).

The electrospray ionization mass spectra (positive mode,  $m/z$  up to  $1200 \text{ amu}$ ) of complex **1** are recorded in methanolic solution (Figure S3). Complex **1** exhibits two major peaks at  $m/z = 452.0020 \text{ amu}$  and  $m/z = 373.9880 \text{ amu}$  for the species  $[\text{C}_{14}\text{H}_{18}\text{BrCuKN}_3\text{O}]^+$  and  $[\text{C}_{14}\text{H}_{18}\text{BrCuN}_2\text{O}]^+$ , respectively (calculated  $m/z$   $452.9622 \text{ amu}$  and  $373.9786 \text{ amu}$ , respectively).

**Crystal Structure Description.** The reaction of CuCl<sub>2</sub> with **HL** in the presence of NaN<sub>3</sub> yields an end-to-end azide-bridged polymeric Cu(II) complex (complex **1**) having the structural formula  $[\text{Cu}(\text{L})(\mu_{1,3}\text{-N}_3)]_{\infty}$ . The complex crystallizes in a non-centrosymmetric orthorhombic  $P2_12_12_1$  space group, with the asymmetric unit comprising one deprotonated L ligand, one Cu(II) atom, and one  $\mu_{1,3}$ -azido anion. The absolute configuration of the structural model is clearly defined by the Flack parameter of  $0.017(7)$ .<sup>34</sup>

The Cu(II) center adopts a distorted square pyramidal geometry ( $\tau \sim 0.25$ ),<sup>35</sup> where the four basal positions are occupied by the N(imine), N(amine), O(phenolato) donor atoms of the chelating L ligand, and N3 atom of an azide anion, whereas the nitrogen N6 of a symmetry-related bridging azide residue is located at the axial position. The apical Cu–N6 bond distance ( $2.434(4) \text{ \AA}$ ) is significantly longer with respect to the other three Cu–N bond lengths, which are the range of  $1.956(3)\text{--}2.078(3) \text{ \AA}$ , in good agreement with values found in the literature.<sup>29,30</sup> On the other hand, the Cu–O1 bond length is shorter ( $1.915(3) \text{ \AA}$ ). The Cu center is displaced from the mean basal plane by  $0.16 \text{ \AA}$  toward the apical azide nitrogen. The N3–Cu–N6, N3–Cu–N2, and N1–Cu–O1 bond angles of  $106.03(16)$ ,  $160.95(16)$ , and  $176.37(13)^\circ$ , respectively, are indicative of the distortions from the ideal square pyramidal geometry (Figure 1).

The structural analysis disclosed the formation of one-dimensional (1D) homochiral polymeric chains wrapped

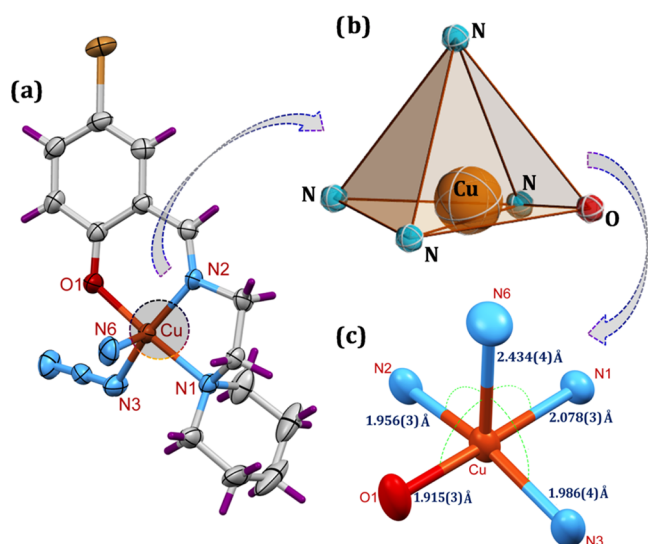


**Figure 1.** (a) ORTEP view of complex **1** with an indication of the metal coordination geometry. (b, c) Polyhedral view around the metal center with a few bond parameters.

around the screw  $2_1$  axis of the right-handed P-helicity, where the chelate conformation at N1/N2 five-membered rings is  $\lambda$ . The chain is composed of copper complexes connected by an end-to-end bridging azide (Figure 2a), with an intermetallic Cu–Cu distance of 6.053 Å. These homochiral chains are connected *via* C–H $\cdots$ N hydrogen bonds (Figure 2b) and, additionally, by CH $\cdots$  $\pi$  interactions to form a two-dimensional network.

Notably, in the case of the complex with a Schiff base lacking bromine, a similar homochiral polymeric chain was obtained, but it was less tightly bound because of an apical Cu–N(azide) distance of ca. 2.8 Å.<sup>36</sup> The hydrogen-bonding parameters and other required bond parameters of complex **1** are tabulated in Tables S3–S5.

**DFT Computation.** To provide theoretical support to the 1D polymer formation of complex **1**, a DFT study was also performed. The molecular structure obtained from the DFT

study clearly shows that the single coordination unit, composed of the N,O-donor-deprotonated ligand and the metal ion, polymerizes through an azido bridge (Figure S4). The TD-DFT calculation is investigated for the validation of the experimental absorption band in the UV–vis spectra. Details of the computational data analysis are discussed in the Supporting Information.

**DNA-Binding Studies.** In the previous section, the synthesis along with the structural description of complex **1** was described. Then, to examine the biomedical application of complex **1**, its DNA-binding efficacy was first investigated thoroughly. Before commencing the work (binding study), it is essential to check the stability of the complex in the working buffer medium. To confirm the stability of the complex in the buffer medium employed, the absorbance of complex **1** as a function of time at a fixed pH was recorded; magnificently, the absorbance of the complex remained unaltered, assuring the stability of the complex in the experimental medium at pH 7.4 (Figure S5). Electronic spectral titration is the most common and important tool to understand the binding efficacy of small molecules with DNA. In this study, actually, the alteration of the absorbance of the studied complex was noted after the incremental addition of ctDNA to it. At the same time, the association constant between complex **1** and the macromolecule was measured; see the Experimental Section. Figure 3 displays the absorbance change of complex **1** after the incremental addition of DNA (10–80  $\mu$ M) to it. Complex **1** exhibits the absorption maxima at 360 nm, which continuously reduces with a 5 nm red shift after the gradual addition of ctDNA to it.

The appearance of an isosbestic point on the titration graph at 382 nm indicates the presence of a strong reversible equilibrium.<sup>37,38</sup> The considerably higher binding constant value of  $2.265 \times 10^5 \text{ M}^{-1}$  suggests the better binding capability of complex **1** with ctDNA. The electronic spectral titration of DNA/HL and the DNA/HL–Cu(II) complex (without the azide) was performed. The titration results are pictographically represented in Figure S6. The titration profile as well as the low binding constant values [ $1.07 \times 10^3 \text{ M}^{-1}$  and  $1.12 \times 10^3 \text{ M}^{-1}$  for HL and HL–Cu(II), respectively] clearly

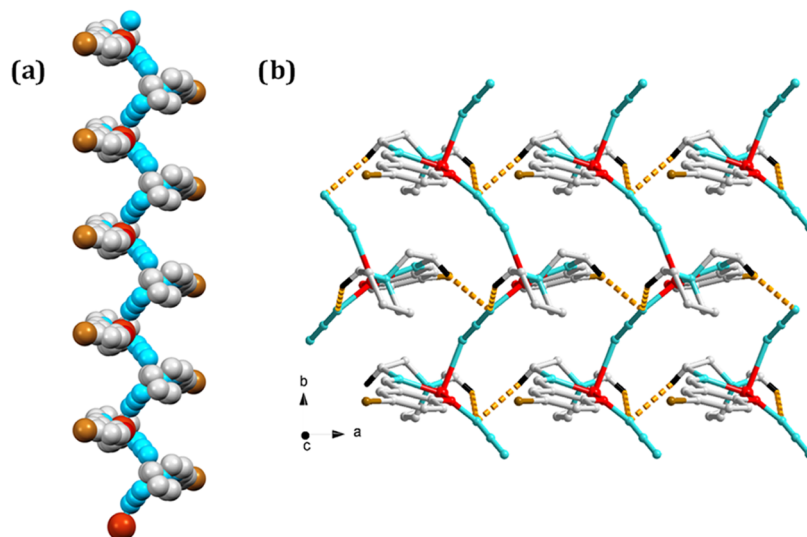


**Figure 2.** (a) 1D zigzag polymeric chain of complex **1** developed along the *b* axis. (b) Two-dimensional (2D) structure of polymeric chains connected by CH $\cdots$ N3 hydrogen bonds, viewed along the crystallographic *c* axis (only H atoms involved in the interactions are indicated).

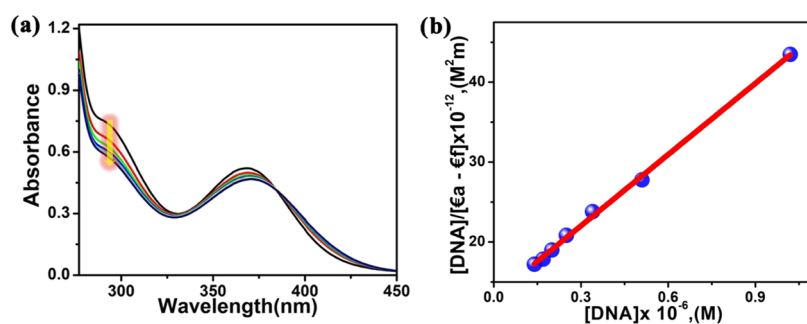


**Figure 3.** (a) Changes in the absorption maxima upon the gradual addition of ctDNA (10–80  $\mu\text{M}$ ) to complex 1. (b) Linear fitting to determine the binding constant.

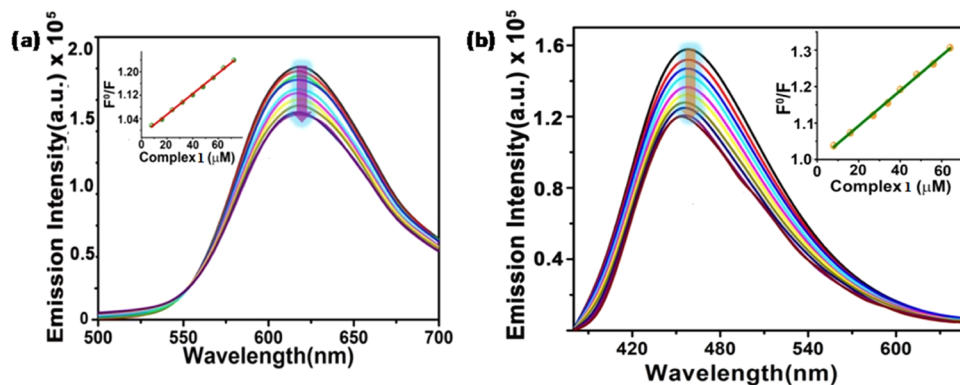


**Figure 4.** Fluorescence intensity changes of (a) EB–DNA and (b) DAPI–DNAs domain after the incremental addition of complex 1 (10–120  $\mu\text{M}$ ). Inset: fluorescence intensity change as a function of the concentration of complex 1 to measure the quenching constant ( $S$ – $V$  plot).

unveil the fact that complex 1 is more susceptible to DNA bonding than precursor compounds such as HL and the HL–Cu(II) complex. The presence of a bulky Br group and a perpendicular azo group in complex 1 favor a partial intercalation along with the groove-binding mode, which is already predicted by the molecular docking study (discussed later).

**Ethidium Bromide (EB) and 4',6-Diamidino-2-phenylindole (DAPI) Displacement Study.** Due to the absence of the photoluminescence property of DNA as well as complex 1, initially, DNA identification was performed by associating it with a fluorophore, and the alteration of the fluorescence intensity of the DNA–fluorophore adduct was recorded after the incremental addition of the studied complex.

In the present study, first, ctDNA–EtBr (intercalator binder) (20  $\mu\text{M}$  + 5  $\mu\text{M}$ ) and ctDNA–DAPI (groove binder) (20  $\mu\text{M}$  + 5  $\mu\text{M}$ ) adducts were formed, and impressively, in the presence of ctDNA, the emission intensity of EtBr and DAPI increases by up to 20-fold due to the strong intercalation and groove binding, respectively.<sup>39–42</sup> In the second step, the emission intensity changes of EtBr–ctDNA/DAPI–ctDNA adducts were recorded after a step-by-step separate addition of complex 1 (10–120  $\mu\text{M}$ ) to the adducts. Interestingly, in every case, a continuous decrease in the emission intensity was visualized after the incremental addition of complex 1 to the adduct (Figure 4). This quenching event can be attributed to the replacement of EtBr or DAPI from the DNA–EtBr/DNA–DAPI moiety with the enhancement of the free EtBr or DAPI molecule concentrations. However, the decrease in the emission intensity can only be reconciled by the efficient interaction potential of complex 1 with DNA, which actually reduces the number of associating parts of DNA available for

DAPI or EtBr. The quenching constant was measured by the Stern–Volmer equation as follows

$$\frac{F_0}{F} = K_{SV}[Q] + 1 \quad (1)$$

where  $F_0$  and  $F$  represent the emission intensity in the absence and presence of the quencher,  $[Q]$  stands for the concentration of the added quencher, and  $K_{SV}$  refers to the quenching constant.<sup>43</sup> From the linear fitting of the curve, the  $K_{SV}$  values were found to be  $2.96 \times 10^4$  and  $3.14 \times 10^4 \text{ M}^{-1}$  for EtBr and DAPI displacement, respectively, suggesting a groove-binding mode along with partial intercalation binding during the association of complex 1 with DNA.

**Viscosity Measurement Study.** The viscosity study is a vital test to obtain typical information regarding the binding mode of the complex to DNA. Hence, before arriving at a conclusion regarding the binding mode of the complex–DNA interaction, the viscosity study should be carried out. Generally, for intercalation binding, the insertion of the compound between the base pair increases the length of DNA, which leads to an enhancement of the viscosity of the bare macromolecule.<sup>44</sup> On the other hand, in the case of groove or other nonclassical modes of binding, the twisting or bending of the double helix leads to a slight reduction of the length of the DNA, as a result of which a slight decrease in the viscosity is observed.<sup>45</sup> Figure S7 clearly displays the relative enhancement of viscosity of the DNA upon incubation with complex 1. Another notable fact is that after the incremental addition of the complex to DNA, the viscosities of the ctDNA–complex 1 adducts increase following a linear pathway, and the pattern of growth follows that observed during DNA–EtBr conjugation. However, the position of the

straight line for the complex–DNA association is at a lower region compared with that of the EtBr–DNA conjugation. This observation suggests that the insertion of complex 1 between the ctDNA base pair is not fully comparable to that of EtBr, a strong intercalator binder. Hence, it can be concluded that the studied complex has the capability to interact with DNA *via* a partial intercalative mode.

**HSA Binding Studies. Electronic Spectral Titration.** The previous section explains well the better association power of complex 1 toward ctDNA, and this investigation is the prime step toward developing a potential anticancer drug. In the next step, we examined the effectiveness of the developed complex toward protein binding. Human serum albumin (HSA) is the most copious protein in the blood plasma, which can play an important role as a drug delivery vehicle carrying the drug molecule to the target location. In the protein-binding study, initially, the UV–vis spectral titration was carried out. In this study, actually, after the incremental addition of complex 1 to HSA (5  $\mu\text{M}$ ), the changes in the absorption were recorded. HSA has a strong absorption at 280 nm, and a continuous enhancement of the absorbance of HSA was visualized after the gradual addition of complex 1 to it (Figure 5). The reason

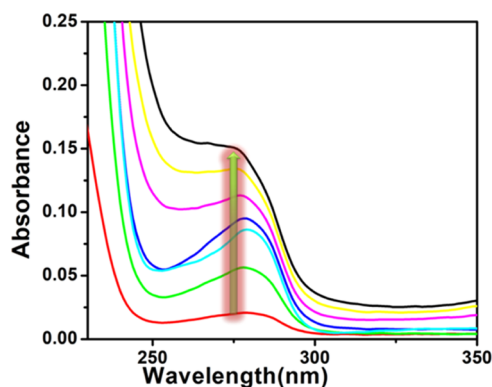


**Figure 5.** Changes in the absorbance of 5  $\mu\text{M}$  HSA with increasing concentrations of complex 1 at 298 K.

behind the enhancement of absorbance is the formation of the ground-state complex with HSA. To avoid the inner filter effect, we modified the spectra using the following equation

$$I = I_{\text{obs}} \times \text{antilog}(A_{\text{ex}} + A_{\text{em}})/2 \quad (2)$$

where  $I$  stands for the corrected intensity and  $I_{\text{obs}}$  represents the observed background-subtracted fluorescence intensity.  $A_{\text{ex}}$  and  $A_{\text{em}}$  correspond to the respective absorbance values measured at excitation and emission wavelengths, respectively.

**Fluorescence-Quenching Studies.** HSA shows an intrinsic luminescence property, mainly due to the presence of two chromophores, namely, tryptophan (Trp) and tyrosine (Tyr). After UV absorption titration, the interaction efficacy of complex 1 with HSA was further studied *via* fluorometric titration. After the gradual addition of complex 1 to HSA, a drastic reduction of the emission intensity of HSA (centered at 340 nm), with a 10 nm spectral shift, was noticed (Figure 6).

We implemented the Stern–Volmer eq 1 to understand the actual quenching mechanism. The double-log plot (Figure 6c) was used to measure the binding constant, and the nature of binding was elucidated by implementing the modified Stern–Volmer plot (Figure 6d)

$$\log \frac{F_0 - F}{F} = \log K + n \log [Q] \quad (3)$$

In the above equation,  $K$  represents the binding constant of the compound with HSA and  $n$  denotes the number of binding sites.

$$\frac{F_0}{F_0 - F} = \frac{1}{f} + \frac{1}{f \times K_Q} \times \frac{1}{Q} \quad (4)$$

Here,  $f$  is the fraction accessible for the protein fluorescence and  $K_Q$  stands for the apparent quenching constant. All of the binding parameters are summarized in Table 1. The value of  $k_q$  (Table 1) is observed to be on the order of  $10^{13}$ , which is found to be higher ( $>10^{12}$ ) than the threshold of  $k_q$  for a typical biomolecular quenching process.<sup>46,47</sup> During the host–guest interaction study, for a diffusion-controlled process followed by a collision (dynamic quenching), the maximum threshold value will be on the order of  $10^{10}$ . Here,  $K_q$  is measured from the relation  $K_q = K_Q / \langle \tau_0 \rangle$ . In the case of static quenching, as  $\langle \tau_0 \rangle$  is controlled by the excited-state property of both the fluorophore and the quencher,  $K_q$  should be higher than  $10^{10}$ .<sup>46</sup> In the present study, the value of  $K_q$  was observed to be higher than the maximum threshold value, which is a signature of a static quenching phenomenon. The  $F_0/F$  vs [complex 1] plot has a straight-line fitting (Figure 6b). Further, to estimate the binding constant, we used the double-log equation eq 3 (Figure 6c), and at the same time, the prediction regarding the nature of binding (static or dynamic) was obtained from the modified Stern–Volmer plot (Figure 6d).

**Circular Dichroism (CD) Spectral Study.** The CD study is a vital tool to assess whether the macromolecules undergo any secondary conformational changes during the interaction with small molecules. In this titration study, the CD spectral changes of bare DNA/HSA in the presence of complex 1 were recorded. Figure 7 clearly depicts a summary of both the CD titration results. The figure shows that the CD spectrum of free DNA represents its canonical b form having a positive lobe at 280 nm and a negative lobe at 248 nm. Interestingly, after the addition of complex 1 to the DNA, very little change in the positive lobe of free DNA was visualized, indicating the retention of the configuration of DNA during the interaction with the studied complex. If the complex is associated with DNA *via* groove binding, one additional hump should generally appear above the 300 nm region, and here, we made the same observation, indicating the groove-binding nature of the complex toward DNA.

Further, Figure 8b shows the CD spectral changes in bare HSA in the presence of complex 1. Free HSA shows two negative peaks at 209 nm ( $\pi \rightarrow \pi^*$  transition) and 220 nm ( $n \rightarrow \pi^*$  transition), representing the  $\alpha$ -helical structure of HSA. After the introduction of the developed complex to HSA, the alteration of the CD spectra was visualized with a slight reduction of its band intensity. The titration profiles were analyzed by utilizing the CD Pro software package. The native HSA  $\alpha$ -helix content of 58.5% was found to be almost constant (57.5%) in the presence of 30  $\mu\text{M}$  complex 1. The observation made from the CD spectral titration profile indicates that complex 1 is unable to modify the conformation of HSA. As the overall style of the curve of HSA before and after the addition of complex 1 does not change, one can easily conclude that the  $\alpha$ -helix remains dominant after the association of HSA with the studied complex.

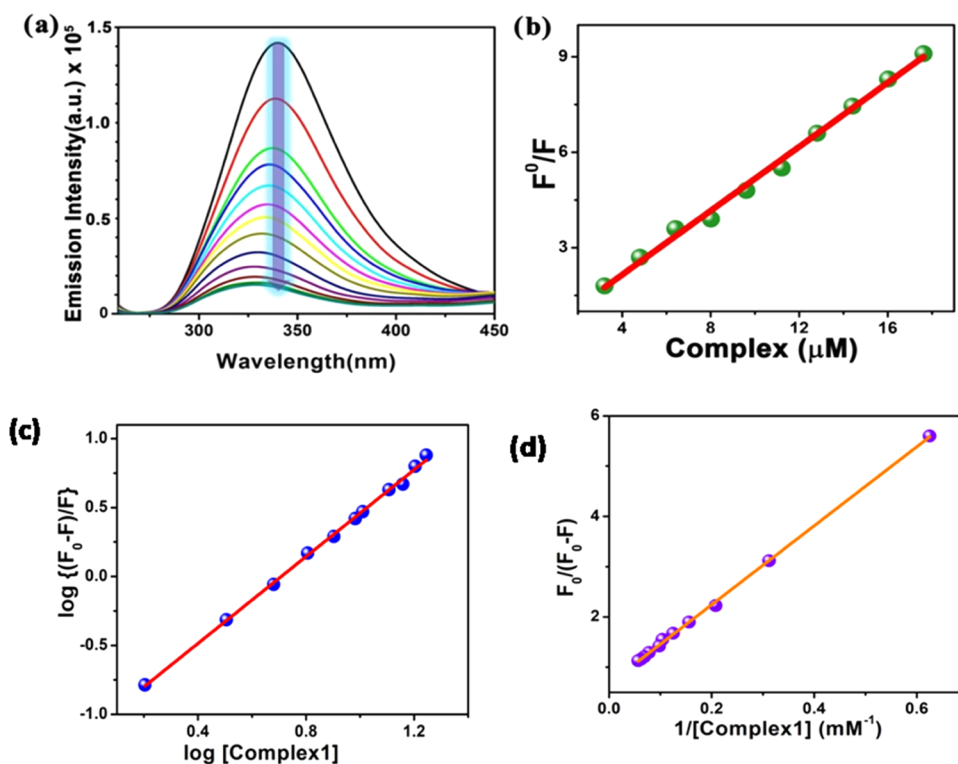


**Figure 6.** (a) Sharp decrease in the HSA (20  $\mu\text{M}$ ) fluorescence intensity after the continuous addition of complex 1 (20–160  $\mu\text{M}$ ). (b) Changes in the fluorescence intensity as a function of the complex concentration to determine the quenching constant. (c) Double-log plot and (d) modified Stern–Volmer plot of HSA with varying concentrations of complex 1.

**Table 1.** Binding Parameters of the HSA-Complex 1 Interaction

sample	$K_b$ ( $\text{L mol}^{-1}$ )	$K_{SV}$ ( $\text{L mol}^{-1}$ )	$k_q$ ( $\text{L mol}^{-1} \text{s}^{-1}$ )	$K_Q$ ( $\text{L mol}^{-1}$ )	$n$
complex 1	$3.28 \times 10^4$	$2.66 \times 10^4$	$4.46 \times 10^{12}$	$3.34 \times 10^4$	0.97

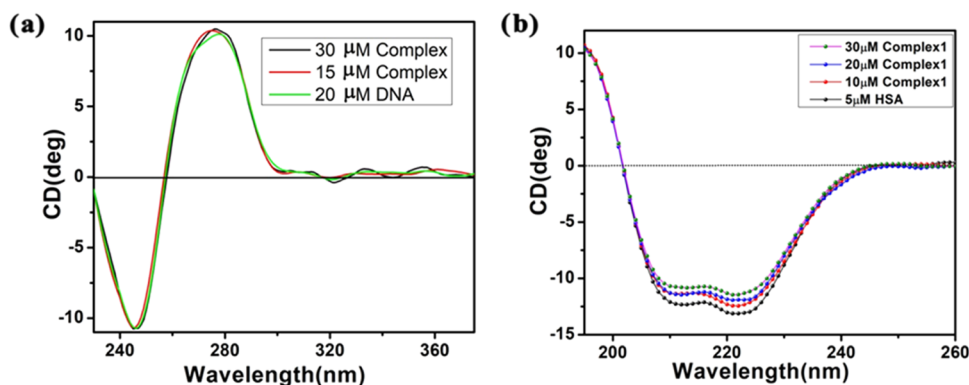


**Figure 7.** CD spectral changes in (a) ctDNA and (b) HSA in the presence and absence of complex 1.

**Lifetime Decay.** To obtain additional proof against the static quenching of HSA in the presence of the quencher complex 1, the lifetime decay measurement study was performed. The characteristic decay profiles and decay parameters for HSA during association with complex 1 are shown in Figure S8 and Table S9, respectively. From the data, it is noticed that both HSA and the HSA–complex adduct show a biexponential decay pattern. The time constant of HSA was calculated to be 1.15 ns, and after the introduction of complex 1 to it, the lifetime of HSA slightly changed from 1.15 ns to 1.23 ns, providing solid proof against the static quenching nature of HSA in the presence of the quencher complex 1. The

observed  $\chi^2$  values in every case for the complex were also found to be well-fitted in the acceptable range.

**Molecular Docking Study.** In fact, before the experimental study, molecular docking was carried out to derive a preliminary idea regarding the binding efficacy of the studied complex with macromolecules, and a range of biophysical studies was performed to obtain experimental validation of the association potential of the complex with macromolecules such as DNA/HSA. Previous reports indicate that 1D azide polymers generally exist as monomeric units in the solution phase. Thus, during the docking study, the mononuclear structure of complex 1 was used, and impressively, the mass

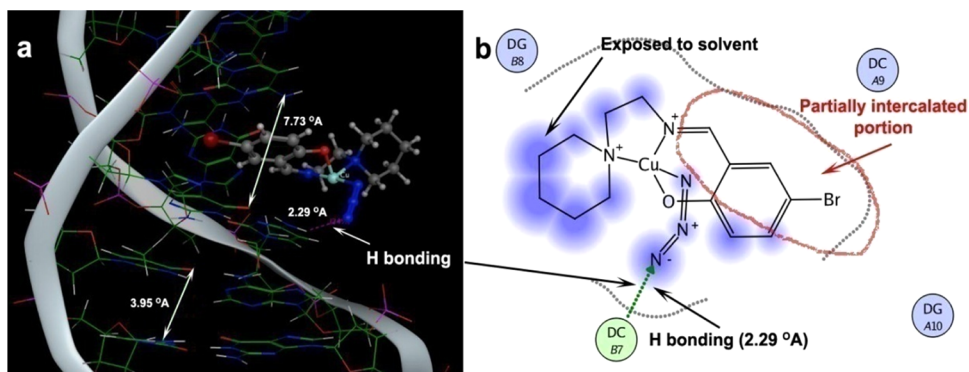


**Figure 8.** (a) Complex 1 bound to DNA via partial intercalation. (b) Two-dimensional image of the binding of the ligand with DNA. Blue spots indicate the portion exposed to the solvent.

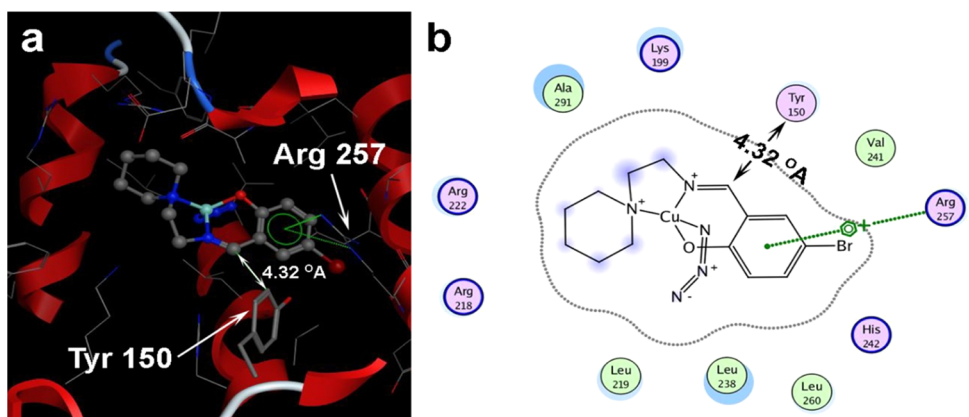


**Figure 9.** (a) Ligand bound to HSA. (b) Two-dimensional image of the ligand bound to HSA, where the dotted line indicates the contour graph of the engulfed portion.

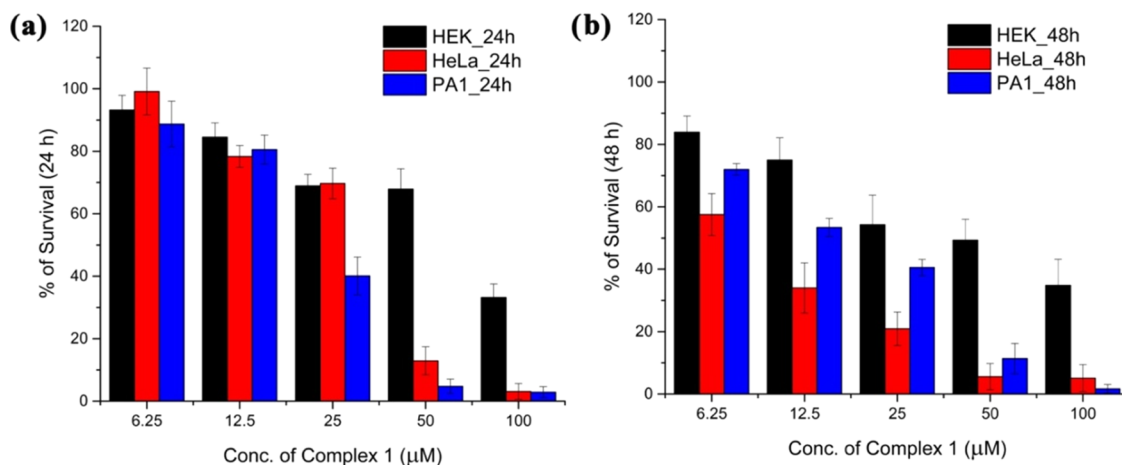


**Figure 10.** Dose-dependent suppression of the cell viability of HeLa, PA1, and HEK cell lines after (a) 24 h and (b) 48 h of incubation for complex 1.

spectral data also yield good support for the existence of a monomeric unit in the solution. In this section, a detailed discussion of the docking study is provided, along with a good match between the experimental and theoretical results. Herein, MOE 2009 software is used for the docking study.<sup>48</sup> The molecular docking study of DNA clearly unveils that the ligand (metal complex) approaches the major groove of the DNA, and its aromatic planar portion partially intercalates into DNA base pairs (Figure 8a).

Generally, a planar ligand can completely intercalate into the base pair of nucleic acids,<sup>49,50</sup> but several pieces of evidence also show partial intercalation visualized due to partial planarity. Here, the studied metal complex lacks planarity due to the presence of a twisted bicyclic piperidine derivative ring. Besides, a triazo group ( $-N=N=N-$ ) that is perpendicularly attached to copper(II) is also responsible for the prevention of full intercalation. However, the perpendicularly present triazo group ( $-N=N=N-$ ) plays a significant role during association with DNA by the formation of

**Table 2. Measured LD<sub>50</sub> Values in Different Cell Lines**

compounds under investigation	cell line	LD <sub>50</sub> _24h (mean ± SD, n = 3)	LD <sub>50</sub> _48h (mean ± SD, n = 3)
complex 1	HEK-293	68.68 ± 5.33	40.80 ± 10.90
complex 1	HeLa	28.46 ± 1.26	7.86 ± 0.57
complex 1	PA1	20.28 ± 0.35	15.23 ± 1.38
CuCl <sub>2</sub>	HeLa	>100	
HL	HeLa	>100	
HL-Cu(II) complex	HeLa	>100	

hydrogen bonds, which gives the metal complex–DNA adduct extra stability. The distance between the base pairs away from the intercalation site is 3.95 Å, whereas this distance increased to 3.73 Å due to partial intercalation of the metal complex. The obtained binding free energy is in the range of −7.98 to −9.12 kcal/mol (binding corresponding to the lowest rmsd is −7.98 kcal/mol), which is in good agreement with that of other studies, related to the DNA-binding efficacy of the metal complex.

The docking study with HSA (Figure 9) reveals that the ligand (metal complex) is completely able to penetrate into the binding site. This study also revealed that arginine (Arg 257) stabilizes the complex by the formation of a positively charged pi interaction with the aromatic ring present in the ligand (metal complex). The fluorescence property of HSA is mainly due to the presence of the aromatic ring-like tyrosine, and the distance between the amino acid and the acceptor ligand is responsible for the fluorescence energy transfer from the amino acid to the ligand. Here, the distance between Tyr150 and the ligand is 4.32 Å, and this distance is suitable for energy transfer (fluorescence quenching in Figure 6). The obtained binding energy (−7.94 kcal/mol) is in good agreement with that of the experimental study.<sup>51,52</sup>

**In Vitro Cytotoxicity Study.** After rigorous inspection regarding the interaction efficacy of complex 1 with the ctDNA/HSA protein, finally, the cytotoxicity assay was performed for its fruitful biomedical implementations. For this purpose, the MTT assay was carried out using two cancer cell lines, namely, human cervical carcinoma (HeLa) and human ovarian carcinoma (PA1) cell lines, and one normal cell line (HEK 293). The dose-dependent cell viability results are shown in Figure 10. The LD<sub>50</sub> values were calculated after 24 and 48 h of incubation of all three cell lines with different doses of complex 1 at 37 °C. During the entire MTT assay, cisplatin was used as the positive control against the HeLa cell line.

Low LD<sub>50</sub> values of complex 1 for HeLa and PA1 cell lines yield strong confirmation of its powerful antiproliferative property with low toxicity toward the normal cell (high LD<sub>50</sub> value obtained for normal HEK cells). For a better understanding, the usefulness of the developed complex 1 was compared with those of several previously reported Cu(II) complexes with respect to effective DNA/protein binding and anticancer activity. A summary of the results of the previously reported Cu(II) complexes is presented in Table S1. The table clearly shows that most of the Cu(II) complexes exhibit effective anticancer properties, which are not only comparable to those of cisplatin but also somehow yield better results. However, in the majority of the cases, protein-binding studies were not reported simultaneously with DNA-binding and anticancer studies. The effects of the previously reported complexes on normal cell lines are also not reported in several cases.

In this present investigation, the antiproliferative property of complex 1 is not only comparable to the effectivity of cisplatin, but it also shows the absence of toxic effects on the normal cell line. In addition, the cytotoxicity of complex 1 toward the two cancer cell lines was found to be much higher than that toward the precursor molecules, *i.e.*, CuCl<sub>2</sub> and the ligand. Interestingly, the IC<sub>50</sub> value of the HL–Cu(II)-only complex (in the absence of azide) is very high in comparison with that of complex 1, and this is displayed in Table 2. This observation clearly unveils the utility of the azide moiety present in complex 1 to exhibit better anticancer properties compared with the HL–Cu(II)-only complex. All of the data given in Table 2 display the selective and specific use of complex 1 as a successful anticancer agent.

**Apoptosis Induced by Complex 1 in a Carcinoma Cell Line.** Finally, to understand the cell death mechanism and to visualize the notable changes within the cell, the nuclear staining technique using different dyes is an unparalleled tool. In this study, in fact, the nuclear and cellular morphological changes of HeLa cells after treatment with complex 1 for 24 and 48 h of incubation with different doses were observed after staining with AO/PI. Figure 11 depicts the nuclear morphological changes after 24 and 48 h of treatment of the cancer cells with different concentrations of complex 1 (12.5, 50 μM).

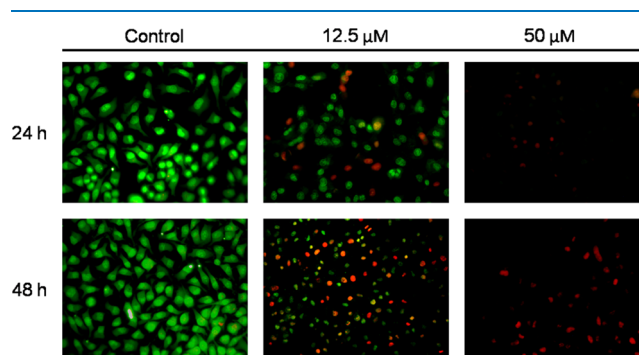


**Figure 11.** HeLa cells stained with AO/PI after treatment with complex 1 for 24 and 48 h.

In controls, cells exhibit green fluorescence showing the unaltered morphology with highly organized nuclei, but with an increasing concentration of the complex, the cell morphology changes and, at the same time, the green fluorescence turns to orange and then red, indicating apoptotic cells with cell shrinkage.<sup>53,54</sup> Thus, after analyzing the results of the staining experiment with the AO/PI strainer, one can conclude that complex 1 triggers apoptosis within the HeLa cell line, causing cellular death.

## CONCLUSIONS

The present work describes the synthesis and thorough identification of a new 1D polymeric Cu(II) complex (**1**), derived from a piperidine-based Schiff base ligand **HL** and anionic azide residue. The single-crystal data analysis as well as density functional theory study show that complex **1** consists of a 1D polymeric structure *via* end-to-end azide bridging. As a preliminary step of the anticancer drug development, complex **1** is inspected to determine its interaction potential with ctDNA and HSA protein. For this purpose, initially, a theoretical study by means of molecular docking was performed, and the results stipulate the binding efficacy of the developed complex toward macromolecules. This theoretical assumption is experimentally validated by implementing a range of biophysical studies. Analyses of steady-state spectral data as well as the displacement assay confirm the partial intercalation mode of complex **1** along with groove-binding toward DNA, and CD spectral titration studies also point out that, during association of the complex with DNA/HSA, no secondary structural changes occur in the macromolecules. These experimental and theoretical studies indicate that the complex can bind with the macromolecules in an effective manner and that the azide group as well as the planar ligand part of the complex play a vital role in the magnificent binding efficacy of the complex. Finally, using the MTT assay, the anticancer activity of complex **1** is analyzed on HeLa and PA1 cancer cell lines as well as on a normal HEK cell line in both dose-dependent and time-dependent manners. The LD50 values recommend complex **1** as a potential anticancer agent with low toxicity to the normal cell. To obtain a preliminary idea regarding the cell-killing mechanism as well as to visualize the morphological changes in HeLa cells after treatment with complex **1**, the AO/PI staining technique was applied, which indicates the occurrence of apoptosis, leading to cancer cell death. Finally, in brief, complex **1** can be effectively implemented for anticancer therapy.

## EXPERIMENTAL SECTION

**Materials and Methods.** All of the reagents and solvents used in this synthesis were commercially available and used without further purifications. 5-Bromo salicylaldehyde, 1-(2-aminoethyl piperidine), ctDNA, HSA, and ethidium bromide (EB) were procured from Sigma Aldrich Chemicals. CuCl<sub>2</sub> and sodium azide (NaN<sub>3</sub>) were purchased from Merck. All interaction studies were performed in citrate–phosphate (CP) buffer of 10 mM [Na<sup>+</sup>] at pH 7.40 containing 0.5 mM Na<sub>2</sub>HPO<sub>4</sub>. Experimental observations (C, H, and N) were recorded using a PerkinElmer 2400II elemental analyzer. An ATR mode Bruker Tensor-27 was used to collect FTIR data. Electronic absorption spectral data were collected using a PerkinElmer UV–Vis Lambda 365 spectrophotometer. All of the fluorometric experiments were conducted using a PerkinElmer fluorescence spectrometer FL6500.

**Synthetic Procedures.** *Synthesis of Ligand HL.* A volume of 0.1 mL (0.7 mmol) of 1-(2-aminoethyl) piperidine was added to a methanolic solution containing 0.140 g (0.7 mmol) of 5-bromo-salicylaldehyde, and after complete addition of the reagents (1:1), the resultant solution was stirred for 3 h.<sup>55</sup> A yellow color developed instantly. The clear yellow-colored solution was directly used for complex preparation.

*Synthesis of [Cu(L)(μ<sub>1,3</sub>-N<sub>3</sub>)]<sub>∞</sub> (1).* Complex **1** was developed by the reaction of an equimolar mixture of the

ligand and the metal salt. A methanolic solution of CuCl<sub>2</sub> (0.11 g, 0.7 mmol) was added *in situ* to the ligand (HL) solution under stirring. After a few minutes, 1.4 mmol of sodium azide was added to it. Then, the resultant solution was stirred for an additional 3 h. After this, the solution was allowed to settle and then filtered. Then, the solution was kept for slow evaporation. After 3 days, small green-colored rectangular crystals were obtained (yield 75%), which were collected and used for further studies. Anal. calcd: for C<sub>14</sub>H<sub>18</sub>BrCuN<sub>5</sub>O (Mw 415.78): C 40.41, H 4.32, N 16.83; found: C 40.36, H 4.23, N 16.62. FT-IR data (KBr pellet): ν(C=N) 1636 cm<sup>-1</sup>, ν(N=N) 2075 cm<sup>-1</sup>, 2032 cm<sup>-1</sup>(skeletal vibration) 1410 cm<sup>-1</sup>, 1310 cm<sup>-1</sup>. UV–vis: 376 nm (CT transition), 650 nm (d–d transition).

*Caution!* Azides are highly explosive and should be handled with proper care.

**X-ray Crystallography.** Single-crystal X-ray diffraction data for complex **1** were collected at room temperature on a Bruker Apex II diffractometer equipped with Mo Kα radiation (λ = 0.71073 Å) and CCD. Cell refinement, data collection, and reduction of the data sets were carried out using the Bruker APEX II and SAINT packages. The appropriate absorption correction was applied with SADABS program.<sup>56</sup> The structure was solved by direct methods<sup>57</sup> and refined using least-squares methods based on F<sup>2</sup> with SHELXL program.<sup>58</sup> In complex **1**, hydrogen atoms were included at calculated positions and non-hydrogen atoms were refined anisotropically. Crystallographic data and refinement parameters of complex **1** are provided in Table 3.

The CIF file of complex **1** has been deposited at the Cambridge Crystallographic Data Centre (CCDC number 2045505). Copies of the data can be obtained, free of charge, on application to the CCDC, 12 Union Road, Cambridge, CB2 1EZ U.K. [Fax: 44 (1233) 336 033; e-mail: [deposit@ccdc.cam.ac.uk](mailto:deposit@ccdc.cam.ac.uk)].

**Theoretical Calculation Method.** All of the calculations were performed at the B3LYP<sup>59,60</sup> level using Gaussian 09 software<sup>61</sup> package. The basis set LanL2DZ was allotted for all of the elements, including metal ions present in the molecule. The ground-state stationary points were entirely optimized at the B3LYP/LanL2DZ level.<sup>62</sup> The electronic excitations based on optimized geometries were calculated using the time-dependent density functional theory (TDDFT) formalism. The Gauss sum<sup>63</sup> was carried out to obtain the theoretical electronic spectra and analyze the influence of the molecular orbital of different structural components in the system.

**Solution Chemistry.** The stability of the complexes in the working buffer solution was confirmed using a UV–vis spectrophotometer. The dimethyl sulfoxide (DMSO) stock solution of complex **1** was added to the CP buffer (pH 7.4), and spectral data were recorded at fixed time gaps.

**DNA/Protein Interaction Studies.** The DNA and HSA stock solutions were prepared by the dilution of ctDNA into a citrate–phosphate (CP) buffer of 10 mM containing 0.5 mM Na<sub>2</sub>HPO<sub>4</sub>. Utilizing the molar extinction coefficient (ε) of 6600 M<sup>-1</sup> cm<sup>-1</sup>, the concentration of DNA was measured spectrophotometrically. During concentration determination in this study, no deviation from the Beer's law was observed.

A fixed concentration of HSA was prepared using the molar extinction coefficient (ε) of 37 500 M<sup>-1</sup> cm<sup>-1</sup>.

The following biophysical experiments were implemented to examine the binding efficacy of DNA/protein with complex **1**.

**Table 3. Crystallographic Data and Refinement Parameters of Complex 1**

	1
CCDC Number	2045505
empirical formula	C <sub>14</sub> H <sub>18</sub> BrCuN <sub>5</sub> O
$f_w$	415.78
crystal size (mm)	0.30 × 0.24 × 0.15
crystal system	orthorhombic
space group	P2 <sub>1</sub> 2 <sub>1</sub> 2 <sub>1</sub>
$a$ (Å)	6.5335(3)
$b$ (Å)	9.5645(5)
$c$ (Å)	26.1697(12)
$\alpha$ (deg)	90
$\beta$ (deg)	90°
$\gamma$ (deg)	90
$V$ (Å <sup>3</sup> )	1635.34(14)
$D_{\text{calcd}}$ (g/cm <sup>3</sup> )	1.689
$Z$	4
$F(000)$	836
$\mu$ (mm <sup>-1</sup> )	3.787
Mo $K\alpha$ radiation	$\lambda = 0.71073$ Å
$T$ (K)	296(2)
$R_{\text{int}}$	0.0642
range of $h, k, l$	−8/8, −12/12, −33/33
$\theta_{\text{min/max}}$ (deg)	2.267/27.162
reflections collected/unique/observed [ $I > 2\sigma(I)$ ]	25433/ 3611/3230
data/restraints/parameters	3611/0/199
GOF on $F^2$	1.060
final	$R_1 = 0.0316$
$R_{\text{indices}}[I > 2\sigma(I)]$	$wR_2 = 0.0751$
$R_{\text{indices}}$ (all data)	$R_1 = 0.0387$
	$wR_2 = 0.0782$
absolute structure parameter	0.017(7)
residuals (e/Å <sup>3</sup> )	0.519, −0.447

**Determination of the Binding Mechanism by a Displacement Assay.** In this study, the fluorescence intensities were recorded after the incremental addition of the complex solution step by step into the ctDNA–EtBr/DAPI domain. HSA is a highly fluorescence-active protein, and the fluorescence titration of HSA was monitored within 250–450 nm upon excitation at 240 nm. Micromolar ( $\mu\text{M}$ ) amounts of stock solutions of complex 1 were added continuously into the adduct, and fluorescence intensity changes were recorded.

**Circular Dichroism Spectral Study.** For the circular dichroism (CD) spectral study, the Jasco J815 model unit (Jasco International Co. Ltd. Hachioji, Japan) was used. In the CD spectral titration, after the addition of increasing concentrations of complex 1 to a fixed concentration of ctDNA/HSA (30  $\mu\text{M}$ ), alterations of the CD spectrum of free DNA/HSA were recorded. Using the equation  $[\theta] = 100 \times \theta / (C \times l)$ , the molar ellipticity values  $[\theta]$  were measured, where  $\theta$  is the observed ellipticity in milli degrees,  $C$  stands for the concentration in mol/L, and  $l$  represents the cell path length of the cuvette in cm. The molar ellipticity  $[\theta]$  (deg cm<sup>2</sup>/dmol) values are represented in terms of base pairs within the region of 200–400 nm.<sup>64</sup>

**Time-Resolved Studies.** Using time-correlated single-photon counting (TCSPC) ( $\lambda_{\text{ex}} = 280$  nm) with a picosecond diode, IBH-NanoLED source N-295, and an fwhm of  $\sim 930$  ps, fluorescence lifetimes were measured. The data were deconvoluted in DAS-6 software and fitted according to the

residuals of fitting function and  $\chi^2$  criteria (neglecting  $\chi^2$  value beyond the range of  $0.99 < \chi^2 < 1.10$ ) using the multi-exponential equation given below:

$$I(t) = \sum \alpha_i e^{-t/\tau_i}$$

$\alpha_i$  denotes the amplitude of the  $i$ th lifetime associated with the  $i$ th lifetime  $\tau_i$ . The average lifetime  $\langle \tau \rangle$  can be calculated as follows:

$$\langle \tau \rangle = \sum \alpha_i \tau_i / \alpha_i$$

**Molecular Docking Studies for DNA Binding and HSA Protein Binding.** All docking studies were performed using MOE 2009 software as mentioned earlier.<sup>65–67</sup> As the actual sequence of ctDNA is unavailable, a DNA crystal (6elb.pdb) was downloaded for further study as a model. For docking with HSA, the crystal structure of the HSA–warfarin complex was downloaded (2bxd.pdb).

To identify the exact site of interaction, the copper complex was placed on a DNA helix, and MD simulation up to 100 ps (interval of 0.5 ps) at 300 K (Supporting Table 1) was run to obtain the most stable complex (lowest energy). Force-field refinement was used throughout the process. A force-field refinement algorithm was used during docking, and a series of binding scores were obtained. The binding score with the lowest root-mean-square deviation (rmsd) was taken as the free energy of binding. For docking with HSA, the same methodology was applied.<sup>65</sup>

**In Vitro Cytotoxicity Assay.** The anticancer activities of complex 1 on the human cervical carcinoma cell line (HeLa) and ovarian cancer cell line (PA1) along with the HEK 293 normal cell line were determined by the traditional MTT assay technique. Cells were seeded at a density of  $2 \times 10^5$  cells/well in a 24-well plate. After 24 h of cell seeding, cells were exposed to complex 1 at different concentrations for 24 and 48 h. After incubation, cells were washed with 1× PBS twice. Then, they were treated with 0.5 mg/mL MTT solution (SRL) and incubated for 3–4 h at 37 °C until a purple-colored formazan product developed. The resulting product was dissolved in DMSO, and the OD was calculated at 570 nm using a microplate reader (Biorad). The rate of survival was determined using the following formula:<sup>68,69</sup>

$$\text{cell viability (\%)} = (\text{OD}_{\text{AT}} / \text{OD}_{\text{AC}}) \times 100$$

where  $\text{OD}_{\text{AT}}$  = absorbance of control cells and  $\text{OD}_{\text{AC}}$  = absorbance of treated cells.

**Acridine Orange (AO) and Propidium Iodide (PI) Dual Staining.** HeLa cells were plated at a density of  $5 \times 10^4$  in 24-well plates with an overnight incubation at 37 °C in a CO<sub>2</sub> incubator. Cells were treated with the desired concentration of complex 1 after 4 h of serum starvation and then incubated at 37 °C for 24 and 48 h. After incubation, the culture medium was aspirated, and cells were washed with 1× phosphate-buffered saline (PBS) twice. The cells were stained with equal volumes (20  $\mu\text{M}$ , AO-PI 1:1) of acridine orange and propidium iodide. The stained cells were kept in the dark for 30 min. The cells were washed once with 1× PBS, and microscopic fluorescence images are obtained.<sup>70,71</sup>

## ■ ASSOCIATED CONTENT

### Supporting Information

The Supporting Information is available free of charge at <https://pubs.acs.org/doi/10.1021/acsomega.2c01403>.

FT-IR, UV–vis spectra, mass spectrum, fluorescence measurements, theoretical calculations, selected bond-angle and bond-length tables and other parameters for complex **1**, lifetime measurement graph, viscosity measurement plot (PDF)

Data\_2 (CIF)

## AUTHOR INFORMATION

### Corresponding Authors

**Somali Mukherjee** – School of Chemical Sciences, Indian Association for the Cultivation of Science, Kolkata 700032 West Bengal, India; [orcid.org/0000-0002-6249-1250](https://orcid.org/0000-0002-6249-1250); Email: [somalimukherjee1993@gmail.com](mailto:somalimukherjee1993@gmail.com)

**Tithi Maity** – Department of Chemistry, Prabhat Kumar College, Contai, Contai 721404, India; [orcid.org/0000-0002-1256-399X](https://orcid.org/0000-0002-1256-399X); Email: [titlipkc2008@gmail.com](mailto:titlipkc2008@gmail.com)

### Authors

**Manik Das** – Department of Chemistry, Prabhat Kumar College, Contai, Contai 721404, India

**Md. Maidul Islam** – Department of Chemistry, Aliah University, Kolkata 700064, India

**Indranil Choudhuri** – Department of Chemistry, Panskura Banamali College, Panskura 721152, India

**Nandan Bhattacharyya** – Department of Chemistry, Panskura Banamali College, Panskura 721152, India

**Bidhan Chandra Samanta** – Department of Chemistry, Mugberia Gangadhar Mahavidyalaya, Purba Medinipur 721425, India; [orcid.org/0000-0002-6029-371X](https://orcid.org/0000-0002-6029-371X)

**Basudeb Dutta** – Department of Chemical Science, IISER Kolkata, Kolkata 741246, India; [orcid.org/0000-0003-4629-5468](https://orcid.org/0000-0003-4629-5468)

Complete contact information is available at: <https://pubs.acs.org/10.1021/acsomega.2c01403>

### Notes

The authors declare no competing financial interest.

## ACKNOWLEDGMENTS

The author Dr. Tithi Maity (T.M.) is extremely grateful to the “West Bengal Science and Technology and Biotechnology, Government of West Bengal” for financial assistance through the scheme Gabesanay Bangla. T.M. acknowledges DST FIST for their financial support to P. K. College, Contai, and expresses deep gratitude to the authority of P. K. College, Contai, for continuous support during the entire period of the work. T.M. is also very thankful to Dr. Partha Pratim Jana, Assistant Professor, Dept. of Chemistry, IIT Kharagpur, for his kind help to collect single-crystal data. The authors are grateful to Professor Ennio Zangrando, Department of Chemical and Pharmaceutical Sciences, University of Trieste, Italy, for his kind help and guidance during the revision of the manuscript, and also express deep gratitude to Prof. Debasis Das, Department of Chemistry, University of Calcutta for the valuable scientific discussion.

## REFERENCES

- (1) Banerjee, S.; Chakravarty, A. K. Metal Complexes of Curcumin for Cellular Imaging, Targeting, and Photoinduced Anticancer Activity. *Acc. Chem. Res.* **2015**, *48*, 2075–2083.
- (2) Galanski, M.; Jakupec, M. A.; Keppler, B. K. Update of the preclinical situation of anticancer platinum complexes: novel design strategies and innovative analytical approaches. *Curr. Med. Chem.* **2005**, *12*, 2075–2094.
- (3) Rosenberg, B.; VanCamp, L.; Trosko, J. E.; Mansour, V. H. Platinum Compounds: a New Class of Potent Antitumor Agents. *Nature* **1969**, *222*, 385–386.
- (4) Qiao, X.; Ma, Z. Y.; Xie, C. Z.; Xue, F.; Zhang, Y. W.; Xu, J. Y.; et al. Study on potential antitumor mechanism of a novel Schiff base copper(II) complex: synthesis, crystal structure, DNA binding, cytotoxicity and apoptosis induction activity. *J. Inorg. Biochem.* **2011**, *105*, 728–737.
- (5) Elsayed, S. A.; Saad, E. A.; Mostafa, S. Development of New Potential Anticancer Metal Complexes Derived from 2-Hydrazinobenzothiazole. *Mini-Rev. Med. Chem.* **2019**, *19*, 913–922.
- (6) Florea, A.-M.; Busselberg, D. Cisplatin as an Anti-Tumor Drug: Cellular Mechanisms of Activity, Drug Resistance and Induced Side Effects. *Cancers* **2011**, *3*, 1351.
- (7) Tadele, K. T.; Tsega, T. W. Schiff Bases and their Metal Complexes as Potential Anticancer Candidates: A Review of Recent Works. *Anticancer Agents Med. Chem.* **2019**, *19*, 1786–1795.
- (8) Rafi, U. M.; Mahendiran, D.; Haleel, A. K.; Nankar, R. P.; Doble, M.; Rahiman, A. K. New pyridazine-based binuclear nickel(II), copper(II) and zinc(II) complexes as prospective anticancer agents. *New J. Chem.* **2016**, *40*, 2451–2465.
- (9) Qi, L.; Lou, Q.; Zhang, Y.; Jia, F.; Zhao, Y.; Wang, F. Advances in Toxicological Research of the Anticancer Drug Cisplatin. *Chem. Res. Toxicol.* **2019**, *32*, 1469–1486.
- (10) Oun, R.; Moussa, Y. E.; Wheate, N. J. The side effects of platinum-based chemotherapy drugs: a review for chemists. *Dalton Trans.* **2018**, *47*, 6645–6653.
- (11) Tsang, R. Y.; Al-Fayea, T.; Au, H. Cisplatin overdose: toxicities and management. *Drug Saf.* **2009**, *32*, 1109–22.
- (12) Jin, J.; Hu, J.; Qin, Y.; Zhang, J.; Zhao, J.; Yue, L.; Hou, H. In vitro and in vivo anticancer activity of a thiourea tripyridyl dinuclear Cu(II) complex. *New J. Chem.* **2019**, *43*, 19286–19297.
- (13) Hasinoff, B. B.; Wu, X.; Yadav, A. A.; Patel, D.; Zhang, H.; Wang, D.; Chen, Z.; Yalowch, J. C. Cellular mechanisms of the cytotoxicity of the anticancer drug elesclomol and its complex with Cu(II). *Biochem. Pharmacol.* **2015**, *93*, 266–276.
- (14) Shi, X.; Chen, Z.; Wang, Y.; Guo, Z.; Wang, X. Hypotoxic copper complexes with potent anti-metastatic and anti-angiogenic activities against cancer cells. *Dalton Trans.* **2018**, *47*, 5049–5054.
- (15) Gupte, A.; Mumper, R. J. Elevated copper and oxidative stress in cancer cells as a target for cancer treatment. *Cancer Treat. Rev.* **2009**, *35*, 32–46.
- (16) Tisato, F.; Marzano, C.; Porchia, M.; Pellei, M.; Santini, C. Copper in diseases and treatments, and copper-based anticancer strategies. *Med. Res. Rev.* **2010**, *30*, 708–749.
- (17) Balsa, L. M.; Ferraresi-curotto, V.; lavecchia, M.; Echeverria, G. A.; Piro, O. E.; Garcia-Tojal, J.; Pis-diez, R.; Gonzalez-Baro, A. C.; Leon, L. Anticancer activity of a new copper(II) complex with a hydrazone ligand. Structural and spectroscopic characterization, computational simulations and cell mechanistic studies on 2D and 3D breast cancer cell models. *Dalton Trans.* **2021**, *50*, 9812–9826.
- (18) Santini, C.; Pellei, M.; Gandin, V.; Porchia, M.; Tisato, F.; Marzano, C. Advances in Copper Complexes as Anticancer Agents. *Chem. Rev.* **2014**, *114*, 815–862.
- (19) Ruiz-Azuara, L.; Gomez, M. E. B. Copper compounds in cancer chemotherapy. *Curr. Med. Chem.* **2010**, *17*, 3606–3615.
- (20) Tabassum, S.; Amir, S.; Arjmand, F.; Pettinary, C.; Marchetti, R.; Masciocchi, N.; Lupidi, G.; Pettinary, R. Mixed-ligand Cu(II)–vanillin Schiff base complexes; effect of coligands on their DNA binding, DNA cleavage, SOD mimetic and anticancer activity. *Eur. J. Med. Chem.* **2013**, *60*, 216–232.
- (21) Zuo, J.; Bi, C.; Fan, Y.; Buak, D.; Nardon, C.; Daniel, K. G.; Dou, Q. P. Cellular and computational studies of proteasome inhibition and apoptosis induction in human cancer cells by amino acid Schiff base–copper complexes. *J. Inorg. Biochem.* **2013**, *118*, 83–93.

- (22) Fousiamol, M. M.; Sithambaresan, M.; Damodaran, K. K.; Prathapachandra Kurup, M. R. Syntheses, spectral aspects and biological studies of bromide and azide bridged box dimer copper(II) complexes of an NNO donor aroylhydrazone. *Inorg. Chim. Acta* **2020**, *501*, No. 119301.
- (23) Pages, B. J.; Ang, D. L.; Wright, E. P.; Aldrich-Wright, J. R. Metal complex interactions with DNA. *Dalton Trans.* **2015**, *44*, 3505–3526.
- (24) Komor, A. C.; Barton, B. K. The path for metal complexes to a DNA target. *Chem. Commun.* **2013**, *49*, 3617–3630.
- (25) Sahabadi, N.; Mohammadi, S. Synthesis Characterization and DNA Interaction Studies of a New Zn(II) Complex Containing Different Dinitrogen Aromatic Ligands. *Bioinorg. Chem. Appl.* **2012**, *2012*, No. 571913.
- (26) Bal-demirci, T.; Congur, G.; Erdem, A.; Erdem-Kurika, S.; Ozdemir, N.; Akgun-Dar, K.; Varor, B.; Ulkuseven, B. Iron(III) and nickel(II) complexes as potential anticancer agents: synthesis, physicochemical and structural properties, cytotoxic activity and DNA interactions. *New J. Chem.* **2015**, *39*, 5643–5653.
- (27) Muenzner, J. K.; Rehm, T.; Biersack, B.; Casini, A.; De Graaf, I. A. M.; Worawutputtpong, P.; Noor, A.; Kempe, R.; Bravec, B.; Kasperkova, J.; Schobert, R. Adjusting the DNA Interaction and Anticancer Activity of Pt(II) N-Heterocyclic Carbene Complexes by Steric Shielding of the Trans Leaving Group. *J. Med. Chem.* **2015**, *58*, 6283–6292.
- (28) Zhou, C. Y.; Zhao, J.; Wu, Y.; Yin, C. X.; Yang, P. Synthesis, characterization and studies on DNA-binding of a new Cu (II) complex with N1, N8-bis (1-methyl-4-nitropyrrole-2-carbonyl) triethylenetetramine. *J. Inorg. Biochem.* **2007**, *101*, 10–18.
- (29) Yinhu, D.; Forougi, M. M.; Boroujeni, Z. A.; Jahani, S.; hani, F.; Rohani, M.; Dusek, M.; Eigner, V.; et al. The synthesis, characterization, DNA/BSA/HSA interactions, molecular modeling, antibacterial properties, and in vitro cytotoxic activities of novel parent and niosome nano-encapsulated Ho(III) complexes. *RSC Adv.* **2020**, *10*, 22891–22908.
- (30) Banerjee, A.; Mohanty, M.; Lima, S.; Samanta, R.; Garribba, E.; Sasamori, T.; Dinda, R. Synthesis, structure and characterization of new dithiocarbamate-based mixed ligand oxidovanadium(IV) complexes: DNA/HSA interaction, cytotoxic activity and DFT studies. *New J. Chem.* **2020**, *44*, 10946–10963.
- (31) Ndagi, U.; Mhlongo, N.; Soliman, M. E. Metal complexes in cancer therapy – an update from drug design perspective. *Drug Des., Dev. Ther.* **2017**, *11*, 599–616.
- (32) Das, K.; Datta, A.; Nandi, S.; Mane, S. B.; Mondal, S.; Massera, C.; Sinha, S.; Hung, C.; Askun, T.; Celikboyun, P.; Cantürk, P.; Garribba, E.; Akitsu, T. A Ni(II) dinuclear complex bridged by end-on azide-N and phenolate-O atoms: spectral interpretation, magnetism and biological study. *Inorg. Chem. Front.* **2015**, *2*, 749–762.
- (33) Thamilarasan, V.; Jayamani, A.; Sengottuvelan, N. Synthesis, molecular structure, biological properties and molecular docking studies on Mn<sup>II</sup>, Co<sup>II</sup> and Zn<sup>II</sup> complexes containing bipyridine–azide ligands. *Eur. J. Med. Chem.* **2015**, *89*, 266–278.
- (34) Spek, A. L. Single-crystal structure validation with the program PLATON. *J. Appl. Crystallogr.* **2003**, *36*, 7–13.
- (35) Addison, A. W.; Rao, N. T.; Reedijk, J.; van Rijn, J.; Verschoor, G. C. Synthesis, structure, and spectroscopic properties of copper(II) compounds containing nitrogen–sulphur donor ligands; the crystal and molecular structure of [1,7-bis(N-methylbenzimidazol-2'-yl)-2,6-dithiaheptane]copper(II) perchlorate. *J. Chem. Soc., Dalton Trans.* **1984**, 1349–1356.
- (36) Das, M.; Mukherjee, S.; Koley, B.; Choudhury, I.; Bhattacharyya, N.; Roy, P.; Samanta, B. C.; Barai, M.; Maity, T. Developing novel zinc (ii) and copper (ii) Schiff base complexes: combined experimental and theoretical investigation on their DNA/protein binding efficacy and anticancer activity. *New J. Chem.* **2020**, *44*, 18347–18364.
- (37) Li, P.; Niu, M.; Hong, M.; Cheng, S.; Dou, J. Effect of structure and composition of nickel(II) complexes with salicylidene Schiff base ligands on their DNA/protein interaction and cytotoxicity. *J. Inorg. Biochem.* **2014**, *137*, 101–108.
- (38) Anam, F.; Abbas, A.; Lo, K. M.; Hameed, S.; Naseer, M. M. Homologous 1, 3, 5-triarylpyrazolines: synthesis, CH $\cdots$  $\pi$  interactions guided self-assembly and effect of alkyloxy chain length on DNA binding properties. *New J. Chem.* **2014**, *38*, 5617–5625.
- (39) Boger, D. L.; Fink, B. E.; Brunette, S. R.; Tse, W. C.; Hedrick, M. P. A simple, high-resolution method for establishing DNA binding affinity and sequence selectivity. *J. Am. Chem. Soc.* **2001**, *123*, 5878–5891.
- (40) Kumar, P.; Gorai, S.; Kumar, M.; Mondal, B.; Manna, D. DNA binding, nuclease activity and cytotoxicity studies of Cu(II) complexes of tridentate ligands. *Dalton Trans.* **2012**, *41*, 7573–7581.
- (41) Eriksson, S.; Kim, S. K.; Kubista, M.; Norden, B. Binding of 4',6-diamidino-2-phenylindole (DAPI) to AT regions of DNA: Evidence for an allosteric conformational change. *Biochemistry* **1993**, *32*, 2987–2998.
- (42) Baguley, B. C.; Bret, M. L. Quenching of DNA-ethidium fluorescence by amsacrine and other antitumor agents: a possible electron-transfer effect. *Biochemistry* **1984**, *23*, 937–943.
- (43) Morgan, A. R.; Lee, J. S.; Pulleyblank, D. E.; Murray, N. L.; Evans, D. H. Ethidium fluorescence assays. Part I. Physicochemical studies. *Nucleic Acids Res.* **1979**, *7*, 547–565.
- (44) Garcia-Gimenez, J. L.; Gonzalez-Alvarez, M.; LiuGonzalez, M.; Macias, B.; Borrás, J.; Alzuet, G. J. Toward the metal based development of metal based synthetic nucleases: DNA binding and oxidative DNA cleavage of a mixed copper (II) complex with N-(9H-Purin-6-yl) benzenesulphonamide and 1, 10-phenanthroline. Antitumor activity in human Caco-2 cells and Jurkat T lymphocytes. Evaluation of P53 and Bcl-2 proteins in the apoptotic mechanism. *Inorg. Biochem.* **2012**, *103*, 923–934.
- (45) Zhang, S.; Yang, H.; Zhao, L.; Gan, R.; Tang, P.; Sun, Q.; et al. Capecitabine as a minor groove binder of DNA: molecular docking, molecular dynamics, and multi-spectroscopic studies. *J. Biomol. Struct. Dyn.* **2019**, *37*, 1451–1463.
- (46) Lakowicz, J. R. *Principles of Fluorescence Spectroscopy*, 3rd ed.; Plenum: New York, 2006.
- (47) Pramanik, U.; Khamari, L.; Shekhar, S.; Mukherjee, S. On the Role of Hydrophobic Interactions between Chloramphenicol and Bovine Pancreatic Trypsin: The Effect of a Strong Electrolyte. *Chem. Phys. Lett.* **2020**, *742*, No. 137137.
- (48) Haque, R.; Mohammad, M.; Islam, M. M. Molecular Docking an Important Tool for Drug Designing. In *Modern Approaches in Drug Designing*; Crimson Publishers, 2018; Vol. 1, pp 1–9.
- (49) Balou, S.; Zarkadoulas, A.; Koukouvitaki, M.; Marchio, L.; Efthimiadou, E. K.; Mitsopoulou, C. A. Synthesis, DNA-Binding, Anticancer Evaluation, and Molecular Docking Studies of Bishomoleptic and Trisheteroleptic Ru-Diimine Complexes Bearing 2-(2-Pyridyl)-quinoxaline, *Bioinorg. Chem. Appl.* **2021**, DOI: 10.1155/2021/5599773.
- (50) Sinha, R.; Islam, M. M.; Bhadra, K.; Suresh Kumar, G.; Banerjee, A.; Maiti, M. The binding of DNA intercalating and non-intercalating compounds to A-form and protonated form of poly(rC)·poly(rG): Spectroscopic and viscometric study. *Biorg. Med. Chem.* **2006**, *14*, 800–814.
- (51) Islam, M. M.; Roy Chowdhury, S.; Suresh Kumar, G. Spectroscopic and calorimetric studies on the binding of alkaloids berberine, palmatine and coralyne to double-stranded RNA polynucleotides. *J. Phys. Chem. B* **2009**, *113*, 1210–1224.
- (52) Bhadra, K.; Suresh Kumar, G.; Das, S.; Islam, M. M.; Maiti, M. Protonated structures of naturally occurring deoxyribonucleic acids and their interaction with berberine. *Biorg. Med. Chem.* **2005**, *13*, 4851–4863.
- (53) Rajendiran, V.; Karthik, R.; Palaniandavar, M.; Stoekli-Evans, H.; Periasamy, V. S.; Akbarsha, M. A.; Srinag, B. S.; Krishnamurthy, H. Mixed-Ligand Copper(II)-phenolate Complexes: Effect of Coligand on Enhanced DNA and Protein Binding, DNA Cleavage, and Anticancer Activity. *Inorg. Chem.* **2007**, *46*, 8208–8221.

- (54) Qiao, X.; Ma, Z. Y.; Shao, J.; Bao, W. G.; Xu, J. Y.; Qiang, Z. Y.; Lou, J. S. Biological evaluation of a cytotoxic 2-substituted Benjimidazole Cu(II) complex: DNA damage, Antiproliferation and apoptotic induction activity in human cervical cancer cell. *BioMetals* **2014**, *27*, 155–172.
- (55) Zhu, X. W.; Yin, Z. G.; Li, G. S.; Yang, X. Z.; Zhang, C. X. {4-Bromo-2-[2-(piperidin-1-ium-1-yl)ethyliminomethyl]phenolato}-diiodidozinc(II). *Acta Crystallogr., Sect. E: Struct. Rep. Online* **2009**, m1226–m1227.
- (56) Bruker. APEX2, SAINT; Bruker AXS Inc.: Madison, Wisconsin, USA, 2012.
- (57) Sheldrick, G. M. *SADABS, Program for Empirical Absorption Correction of Area Detector Data*; University of Gottingen: Germany, 1996.
- (58) Sheldrick, G. M. *SHELX-a program for automatic solution of crystal structures*; University of Gottingen: Germany, 1997.
- (59) Frisch, M. J.; Trucks, G. W.; Schlegel, H. B.; Scuseria, G. E.; Robb, M. A.; Cheeseman, J. R.; Scalmani, G.; Barone, V.; Mennucci, B.; Petersson, G. A.; Nakatsuji, H.; Caricato, M.; Li, X.; Hratchian, H. P.; Izmaylov, A. F.; Bloino, J.; Zheng, G.; Sonnenberg, J. L.; Hada, M.; Ehara, M.; Toyota, K.; Fukuda, R.; Hasegawa, J.; Ishida, M.; Nakajima, T.; Honda, Y.; Kitao, O.; Nakai, H.; Vreven, T.; Montgomery, J. A., Jr.; Peralta, J. E.; Ogliaro, F.; Bearpark, M.; Heyd, J. J.; Brothers, E.; Kudin, K. N.; Staroverov, V. N.; Kobayashi, R.; Normand, J.; Raghavachari, K.; Rendell, A.; Burant, J. C.; Iyengar, S. S.; Tomasi, J.; Cossi, M.; Rega, N.; Millam, J. M.; Klene, M.; Knox, J. E.; Cross, J. B.; Bakken, V.; Adamo, C.; Jaramillo, J.; Gomperts, R.; Stratmann, R. E.; Yazyev, O.; Austin, A. J.; Cammi, R.; Pomelli, C.; Ochterski, J. W.; Martin, R. L.; Morokuma, K.; Zakrzewski, V. G.; Voth, G. A.; Salvador, P.; Dannenberg, J. J.; Dapprich, S.; Daniels, A. D.; Farkas, O.; Foresman, J. B.; Ortiz, J. V.; Cioslowski, J.; Fox, D. J. *Gaussian 09*, revision D.01; Gaussian Inc: Wallingford, CT, 2009.
- (60) Becke, A. D. Density-functional thermochemistry. III. The role of exact exchange. *J. Chem. Phys.* **1993**, *98*, 5648–5652.
- (61) Cossi, M.; Barone, V. Time-dependent density functional theory for molecules in liquid solutions. *J. Chem. Phys.* **2001**, *115*, 4708–4717.
- (62) Cossi, M.; Rega, N.; Scalmani, G.; Barone, V. Energies, structures, and electronic properties of molecules in solution with the C-PCM solvation model. *J. Comput. Chem.* **2003**, *24*, 669–681.
- (63) O'Boyle, N. M.; Tenderholt, A. L.; Langner, K. M. cclib: a library for package-independent computational chemistry algorithms. *J. Comput. Chem.* **2008**, *29*, 839–845.
- (64) Gradinaru, J.; Forni, A.; Druta, V.; Tessore, F.; Zecchin, S.; Quici, S.; Garbalau, N. Structural, Spectral, Electric-Field-Induced Second Harmonic, and Theoretical Study of Ni(II), Cu(II), Zn(II), and VO(II) Complexes with [N2O2] Unsymmetrical Schiff Bases of S-Methylisothiosemicarbazide Derivatives. *Inorg. Chem.* **2007**, *46*, 884.
- (65) Khan, S.; Masum, A. A.; Giri, P.; Islam, M. M.; Harms, K.; Chattopadhyay, S. Chirality-Induced Variation in Interaction of Two Similar Copper(II) Coordination Polymers with Calf Thymus DNA: Exploration of Their Antimicrobial Activity and Cytotoxicity. *ChemistrySelect* **2018**, *3*, 7112–7122.
- (66) Zhang, J.; Gao, X.; Huang, J.; Wang, H. Probing the Interaction between Human Serum Albumin and 9-Hydroxyphenanthrene: A Spectroscopic and Molecular Docking Study. *ACS OMEGA* **2020**, *5*, 16833–16840.
- (67) Nayim, S.; Jana, G. C.; Aktara, M. N.; Khatun, M.; Das, S.; Islam, M. M.; Jha, P. K.; Hossain, M. Berberine derivatives as heteroatom induced hydrophobic sensor: An analytical approach for the selective and sensitive fluorometric detection and discrimination of serum albumins. *Anal. Chim. Acta* **2019**, *1065*, 124–133.
- (68) Mosmann, T. Rapid colorimetric assay for cellular growth and survival: Application to proliferation and cytotoxicity assays. *J. Immunol. Methods* **1983**, *65*, 55–63.
- (69) Kwan, Y. P.; Saito, T.; Ibrahim, D.; Al-Hassan, F. M. S.; Oon, C. E.; Chen, Y.; Jothy, S. L.; Kanwar, J. R.; Sasidharan, S. Evaluation of the cytotoxicity, cell-cycle arrest, and apoptotic induction by *Euphorbia hirta* in MCF-7 breast cancer cells. *Pharm. Biol.* **2016**, *54*, 1223–1236.
- (70) Alherby, L.; Pandurangan, S. B.; Binobead, M. A.; Alhussain, M.; et al. Potential Metabolite Nymphayol Isolated from Water Lily (*Nymphaea stellata*) Flower Inhibits MCF-7 Human Breast Cancer Cell Growth via Upregulation of Cdkn2a, pRb2, p53 and Down-regulation of PCNA mRNA Expressions. *Metabolites* **2021**, *10*, 280.
- (71) Zhang, J.; Ming, C.; Zhang, W.; Okechukwu, P. N. 10H-3,6-Diazaphenothiazine induces G2/M phase cell cycle arrest and caspase-dependent apoptosis and inhibits cell invasion of A2780 ovarian carcinoma cells through the regulation of NF-κB and (BIRC6-XIAP) complexes. *Drug Des., Dev. Ther.* **2017**, *11*, 3045–3063.